New Time-Domain EPR Methods for the Study of Slow Motions on Surfaces

Glenn L. Millhauser, Jeff Gorcester, and Jack H. Freed
Baker Laboratory of Chemistry, Cornell University, Ithaca, New York 14853, USA

Abstract

Cw-EPR studies of slow motions of paramagnetic species on surfaces are likely to lead to ambiguous results because there are only residual motional effects in the spectrum but significant inhomogeneous broadening due to site variations. Recently developed time-domain experiments which substantially overcome such difficulties are reviewed. In the first, one obtains a graph of the variation of T_2 across the spectrum, from which the model for reorientation of spin species can be inferred. In another example, one obtains the variation of the magnetization-transfer rate T_A^{-1} across the spectrum, which leads in the case of physisorbed NO_2 to a dramatic indication of anisotropic rotation. These are magnetic-field-swept two-dimensional experiments, but the very recent development of two-dimensional Fourier-Transform techniques is reviewed, since they are expected to be very useful in studies of slow motions. Also, a recent time-domain study of physisorbed H and D atoms is reviewed. It is suggested that the anomalously short temperature-independent and concentration-independent phase memory time is due to surface diffusion by a tunneling mechanism.

I. Introduction

Electron paramagnetic resonance (EPR) spectroscopy has traditionally been a method for the study of molecular motions in condensed phases. The motion of radicals adsorbed on solid surfaces has also been studied by a number of workers. Until recently, such studies were mostly limited to "qualitative" analysis of the EPR spectra in terms of the motion of the radical and the nature of the radical-surface interaction (1–7). However, there were some early efforts at a more "quantitative" analysis of the molecular dynamics based upon EPR lineshape studies (8–10). In the early 1980s, Freed and co-workers performed some detailed studies on motional dynamics on surfaces which included extensive theoretical analysis of the continuous wave (cw) EPR line-

Electronic Magnetic Resonance of the Solid State
Edited by John A. Weil (Associate editors: Michael K. Bowman, John R. Morton, Keith F. Preston).
Published by The Canadian Society for Chemistry, Ottawa, Canada 1987
ISBN: 0-921763-00-X

shapes (11, 12). While these results were quite intriguing, they indicated the difficulty in disentangling dynamic information from the typically broad and inhomogeneous lineshapes characteristic of adsorbed radicals. In fact, there is considerable inhomogeneous broadening due to site variations on the adsorbed surfaces.

Modern electron-spin-echo techniques (13–16) are now beginning to play a useful role in the study of molecular motions. While earlier work focussed largely on measurements of T_1 and T_2, it became clear that for studies of slow motions characteristic of viscous fluids or of species adsorbed on surfaces, time-resolved methods specific to the slow motional regime would be highly desirable. This has now lead to a concurrent development of new theory (17–19) for the effects of modern pulse sequences on the "dynamic spin packets", which constitute the inhomogeneously broadened lines that still contain dynamic information, and of a set of new time-domain experiments for studying these dynamic spin packets (19–23).

In this work we wish to present both a review and a progress report on the current status of the use of these new techniques for the study of slow motions on surfaces. Although these techniques are very recent, there nevertheless has been the opportunity to demonstrate the applicability of some of them to the study of dynamics on surfaces, as we review below. In the authors' estimation, the class of new time-resolved EPR techniques will see rapid development in the next few years, so that we wish to note the newest techniques appropriate for molecular dynamics in general, since these can be expected in the future to apply to studies on surfaces.

In our review we first summarize (Section II) the earlier findings from cw-EPR studies of Freed and co-workers on the motional dynamics of O_2^- chemisorbed on supported surfaces and of NO_2 that is physisorbed. We then describe (Section III) the T_2-type of 2D-experiment (20–23), which provides a slow-motional spectrum plotted as a function of both the swept magnetic field (as in a normal cw *absorption* EPR spectrum) and a frequency or "width." This latter width axis displays the natural (homogeneous) lineshapes occurring at the different resonance positions of the EPR spectrum. A detailed study (22) of the physisorbed NO_2 system is then reviewed to show that much more accurate information on the dynamics is obtained from two-dimensional electron spin echo (2D-ESE) experiments, which has resulted in a new interpretation of the original cw results. We then describe (Section IV) the newer two-dimensional magnetization transfer experiment as applied to the physisorbed NO_2 case (19). Next we review (Section V) our recent experiments (22)

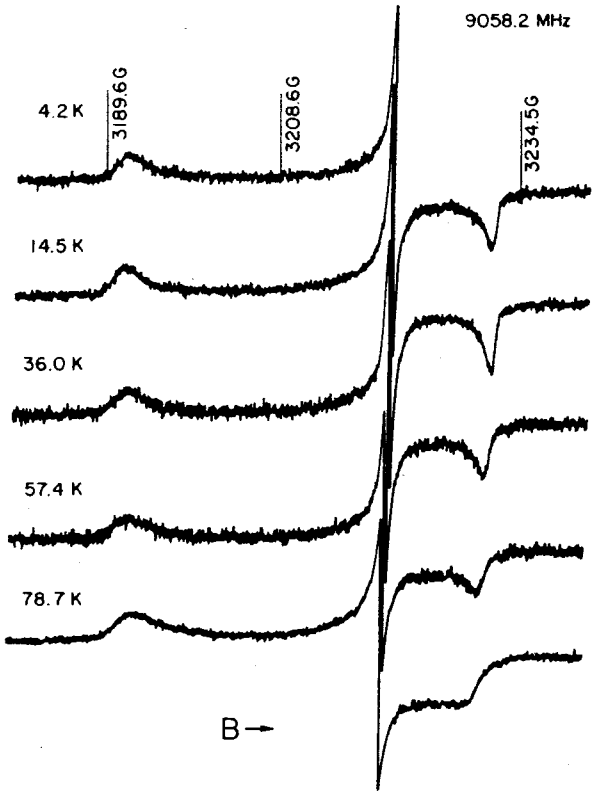

Figure 1. Temperature-dependent X-band EPR spectra of O_2^-(III) on vycor-supported Ti ions [from (11)].

on physisorbed H atoms (by more conventional ESE techniques), since this is an effort to determine the source of the fundamental underlying relaxation on a surface. Last, but not least, we briefly describe (Section VI) the newest two-dimensional Fourier Transform techniques (24), which we believe will revolutionize EPR as applied to the study of slow motions.

II. A Review of Some CW-EPR Studies: O_2^- and NO_2

The O_2^- ion on a variety of surfaces has been extensively studied by a number of workers (7). In particular, Shiotani *et al.* (11) found several types of O_2^- in their experiments on O_2^- adsorbed on Ti ions supported on porous vycor glass.

These could be distinguished by their different g-matrices. The rationalization of these matrices in terms of extended Hückel theory has also been provided more recently (25). For one type of O_2^-, called O_2^-(III), it was observed from studies over the temperature range of 4.2 to 400 K that the line position corresponding to one g-matrix component perpendicular to the internuclear axis of O_2^- remained constant with temperature, whereas the other two principal components of the g-matrix were found to vary with temperature, and were accompanied by drastic lineshape changes (*e.g.*, Figure 1). This observation strongly suggested that there is molecular motion of this O_2^- on the surface and that this motion is highly anisotropic, consisting essentially of planar rotation about the axis simultaneously perpendicular to the internuclear axis of O_2^- and parallel to the normal to the surface. It appeared that this motion was even occurring at very low temperatures (*ca.* $T \lesssim 15$ K; cf. Figure 1). The EPR lineshapes were simulated according to slow-motional lineshape theory for different possible models. While a model of weak-jump planar diffusion seemed to provide the best fit to the observed spectra, there were significant discrepancies between this theory and the experiment.

In a closely related work, NO_2 adsorbed on crushed vycor glass (and on a zeolite) was studied by EPR over a comparable wide range of temperature. Similar, though less dramatic, observations were made; *viz.* (1) the lineshapes change with temperature; (2) the low-temperature ($T \lesssim 77$ K) rotational motion of NO_2 is described by a diffusion tensor that is axially symmetric about the molecular y-axis (*i.e.*, parallel to the O−O internuclear axis) such that motion about this axis is about 10 times faster than that about the x and z axes; (3) motion persists to very low temperatures; (4) there are significant discrepancies between the observed and calculated lineshapes (*cf.* Figure 2).

Once ESE experiments began to be performed, it quickly became clear that the story would most likely have to be modified. Initial measurements obtained from ESE phase-memory times showed T_2 to be about 10 times longer than that derived from the analysis of the cw-EPR spectrum (11), for both cases. This result strongly suggested that the observed cw-EPR linewidth is largely due to inhomogeneous broadening. But then what is the source of its significant temperature dependence? It was suggested (11) that it might be necessary to include residual quantum effects of the rotational motions on the surface. The inhomogeneous broadening could then be due either to site variations of rotational "tunneling" or to different quantum pseudo-rotational states. But simple measurements of T_2 (and T_1) could not provide very extensive data. We turn, therefore to the new 2D-ESE methods.

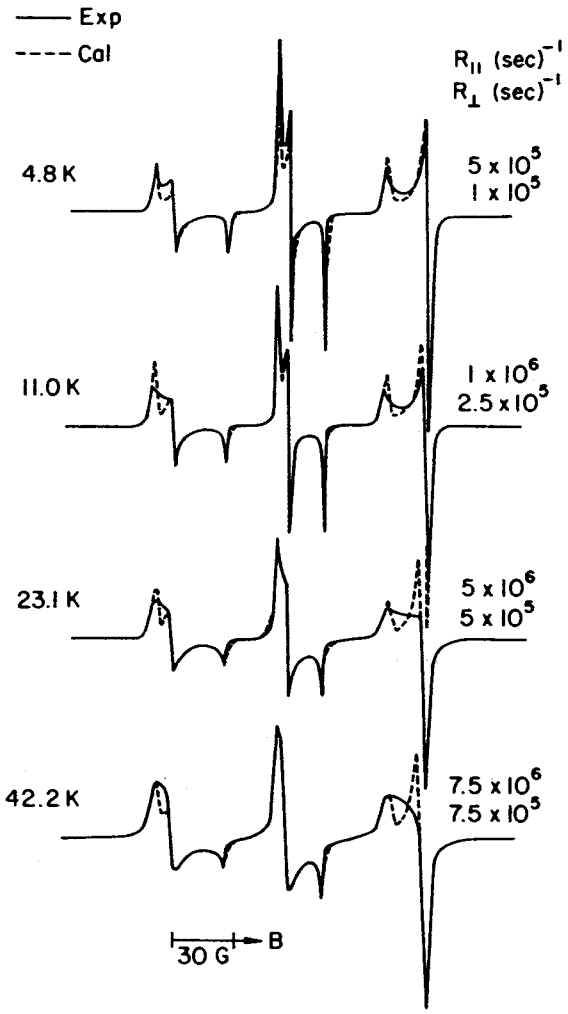

Figure 2. Temperature-dependent X-band EPR spectra of NO_2 on vycor, with best-fitting calculated spectra based on anisotropic Brownian diffusion; $R_{\parallel}$ and $R_{\perp}$ are the parallel and perpendicular rotational diffusion coefficients [from (12)].

III. 2D-ESE Studies of T_2 Variations Across the Spectrum

A) *The Method*

The 2D-ESE method for studying T_2 variations across the spectrum is based

upon a theoretical study of ESE and slow motions by Schwartz *et al.* (17). It was shown that the time evolution of the echo height for slow motions could, in general, be represented as a sum of complex exponentials. That is, the observed echo signal, S at time $2\tau + t$, is given by

$$[1] \qquad S(2\tau + t) = \mathrm{Re} \sum_{l,j} a_{lj} \exp[-(\Lambda_l + \Lambda_j^*)\tau] \exp[-\Lambda_l t],$$

where τ is the time between the $\pi/2$ and π pulses and where $2\tau + t$ is the time period measured from the initial pulse. The echo maximum is expected at time 2τ, and Re represents the real part of the complex function to its right. Equation [1] can best be understood in terms of the concept of the "dynamic spin packet" (DSP). That is, in the rigid limit, the inhomogeneously broadened EPR spectrum from a polycrystalline (or glassy) sample is made up of the broad envelope of contributions from many, many (actually a continuum of) spin packets, each one resonating at a definite frequency and associated with the spins on molecules oriented at the appropriate angle with respect to the static magnetic field. As the rotational motion increases, each spin-packet in the continuum will "interact" with nearby spin-packets, since the motion will transform molecules contributing to one spin-packet into contributors to another at a different orientation. As a result of this coupled behavior of the original (i.e., rigid-limit) spin packets, there will be new "normal-mode" solutions, the DSP's, which will be linear combinations of the original spin packets. The physics of the problem is described by the stochastic Liouville equation, which simultaneously includes the reversible quantum-mechanical spin dynamics and the irreversible molecular dynamics (usually treated classically). The eigenvectors of the stochastic Liouville operator are the DSPs, and the Λ_j in Equation [1] are the corresponding eigenvalues in the rotating frame. The imaginary parts $\mathrm{Im}(\Lambda_j)$ represent the resonance frequencies of the associated DSPs [i.e., $\omega_j \equiv \mathrm{Im}(\Lambda_j)$], while the real parts $\mathrm{Re}(\Lambda_j)$ represent the corresponding natural or homogeneous widths and are associated with the observed $T_{2,j} \equiv [\mathrm{Re}(\Lambda_j)]^{-1}$. (Note that the asterisk in Equation [1] represents a complex conjugation, which requires a simple generalization (17) if echo envelope modulation is to be considered). In general, the relative weights of the DSPs given by the "diagonal" coefficients a_{ll} in [1] and the "beats" between pairs of DSPs given by the "off-diagonal" coefficients a_{lj} ($l \neq j$) have a complicated dependence upon the form of these "normal-modes" and of the spin transition moments as averaged over the equilibrium ensemble of molecular orientations. However, near the rigid limit, the a_{lj} simplify to

[2] $$a_{ij} \cong (\mathbf{O}^T U)_j^2 \, \delta_{ij}$$

where O is the (nearly) real orthogonal matrix associated with the transformation that diagonalizes the stochastic-Liouville operator, while U is the vector of (appropriately averaged) spin transition moments.

When Equation [2] applies, Equation [1] becomes

[3] $$S(2\tau + t) \propto \sum_j a_{jj} \exp[-2\mathrm{Re}(\Lambda_j \tau)] \exp[-\mathrm{Re}(\Lambda_j t)] \cos[\mathrm{Im}(\Lambda_j t)].$$

Thus, in a "two-dimensional" plot of S *vs.* the two independent variables τ and t, the t dependence includes both the resonance frequency of each DSP and its $T_{2,j}$. If we set $t = 0$ and step out τ, then we obtain the echo envelope as a superposition of exponential decays corresponding to the different $T_{2,j}$ values from each DSP contributing appreciably to the signal. However, such a result would be difficult to disentangle. Instead, let us take advantage of the additional resolution provided by two-dimensional spectroscopy. Let us perform a double Fourier Transform (FT) of Equation [3], recognizing however that in the near-rigid limit the linewidth for each DSP will largely be masked by various sources of inhomogeneous broadening such as unresolved super hf interactions and site variations in the spin-Hamiltonian parameters. We shall therefore assume a Gaussian inhomogeneous width $\Delta \gg T_{2,j}^{-1}$. This yields the two-dimensional spectrum given by

[4] $$S(\omega, \omega') \propto \sum_j a_{jj} \frac{T_{2,j}}{1 + \omega^2 T_{2,j}^2} \exp[-(\omega' - \omega_j)^2/\Delta^2],$$

which is a Lorentzian along the ω-axis (the FT of τ) and a Gaussian along the ω'-axis (the FT of t). But more important, we have separated out the role of the relaxation of each spin packet given by its $T_{2,j}$, which is plotted along the ω axis, from its resonance position in the spectrum given along the ω' axis. In fact, for $\omega = 0$ we almost recover the expression for the cw lineshape (with Gaussian inhomogeneous broadening) along the ω'-axis. Thus this separation allows us to *observe how the $T_{2,j}$ values vary across the whole spectrum.* In other words we have succeeded in resolving the different dynamic behavior of the various spin packets, subject however to the resolution limit due to the inhomogeneous broadening, Δ.

The actual experimental technique that has been utilized by Millhauser and Freed (MF) (20) is to sweep through the static magnetic field B_0 very slowly, but with a microwave-field intensity B_1 small enough that only DSPs associated with widths well within the inhomogeneous width Δ are effectively rotated by

the pulses. MF show that Equation [4] applies to their experiment provided that the following set of inequalities applies

$$\gamma B_s > \Delta \gg \gamma B_1 \gg T_{2,j}^{-1} \quad [5]$$

where γB_s is the full extent of the spectrum. In this format, one sweeps through B_0 and observes the echo height at 2τ, *i.e.*, one obtains an "echo-induced EPR spectrum" for each value of τ. This provides an $S(\tau, \omega')$ such that the FT in t is automatically obtained. Then a FT in τ is performed after the experiment is repeated for a sufficient number of values of τ to obtain the form of Equation [4]. This technique has the advantage of simplicity, a minimum of experimental artifacts, and only low-power microwave pulses are required. However, it is time consuming, typically requiring about 5 hrs for a complete set of 2D data.

We shall show in Sect. VI that modern techniques now permit such an experiment to be performed with large enough B_1 pulses such that the whole spectrum can be irradiated. For this newest technique the relevant inequalities would be

$$\gamma B_1 \approx \gamma B_s > \Delta \gg T_{2,j}^{-1} \quad [6]$$

in order that Equation [4] be obtained after a double FT in τ *and* t. This newest technique is much more difficult and is fraught with a variety of instrumental artifacts which must be corrected for. Nevertheless, by removing the need to sweep slowly through B_0, but instead to gather the *whole* spectrum after each echo sequence, at *the least* there is an order-of-magnitude savings in time.

Before closing the summary of this technique we wish to point out that an important experimental artifact has not been included in Equation [4], *viz.* the effect of a non-zero dead-time τ_d after the second pulse (largely due to cavity ringing), so that one is restricted to $\tau \geq \tau_d$. Equation [4] may be corrected for this effect by multiplying by a factor: $\exp[-2\tau_d/T_{2,j}]$ inside the summation. However, more recently Millhauser and Freed (23) have shown that a modern technique of data analysis, *viz.* linear prediction with singular-value decomposition (LPSVD), enables one to back-extrapolate the 2D-ESE data set to estimate the signal in the range $0 < \tau \leq \tau_d$. The LPSVD method is especially important in that it also leads both to significantly improved resolution enhancement of the complex 2D line shapes as well as to the least-squares values characterizing the exponential decays consistent with Equations [3] and [4] (23).

The actual data are most usefully displayed not by the full 2D representation,

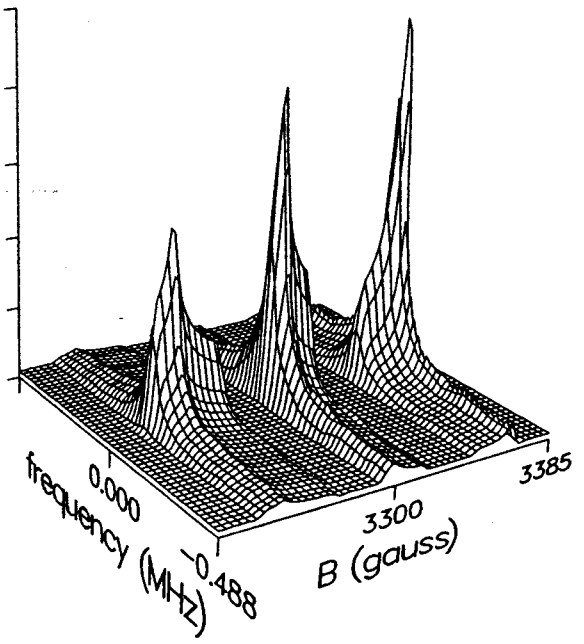

Figure 3. 2D-ESE X-band spectrum from NO_2 on vycor at 5 K [from (22)].

but by normalized contours. These are produced by dividing $S(\omega, \omega')$ by the "zero MHz slice" [*i.e.*, $S(0, \omega')$] to normalize and then to display the constant contour lines. A set of horizontal lines implies that there is no T_2 variation across the spectrum, whereas contour lines with curvature indicate the presence of at least some variation.

In the general theoretical analysis of this experiment, MF show that Brownian reorientation, which occurs by infinitesimal steps, will lead to a T_2 variation, because of the different sensitivity of different spectral regions to a small change in molecular orientation [*i.e.*, $dS(\omega')/d\theta$ varies across the spectrum]. On the other hand, reorientation by substantial jumps does not show any T_2 variation. Another possible contribution to variation in T_2 will be that due to anisotropic diffusion.

B) *An Example of 2D-ESE: NO_2/Vycor*

We show in Figure 3 the 2D-ESE spectrum obtained from the NO_2/vycor system at 5 K (22). The more useful normalized contour plots are shown in Figure 4. The parallel contours in Figure 4a indicate that "T_2" is uniform over

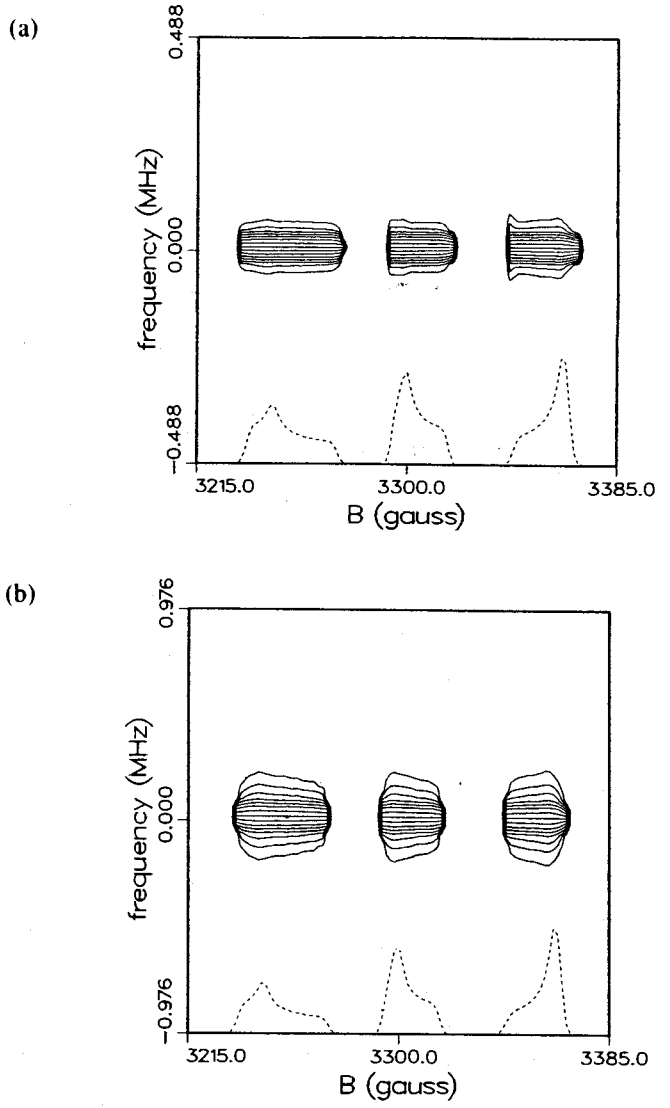

Figure 4. 2D Normalized contour maps (and zero MHz slices) for NO_2 on vycor at a) 5 K, b) 35 K [from (22)].

the inhomogeneously broadened spectrum at 5 K. This situation is not dramatically altered as the temperature is raised to 60 K (*e.g.*, Figure 4b for 35 K). However, a careful analysis of the 2D-ESE results by the LPSVD method, clearly showed that at each temperature these spectra have two dom-

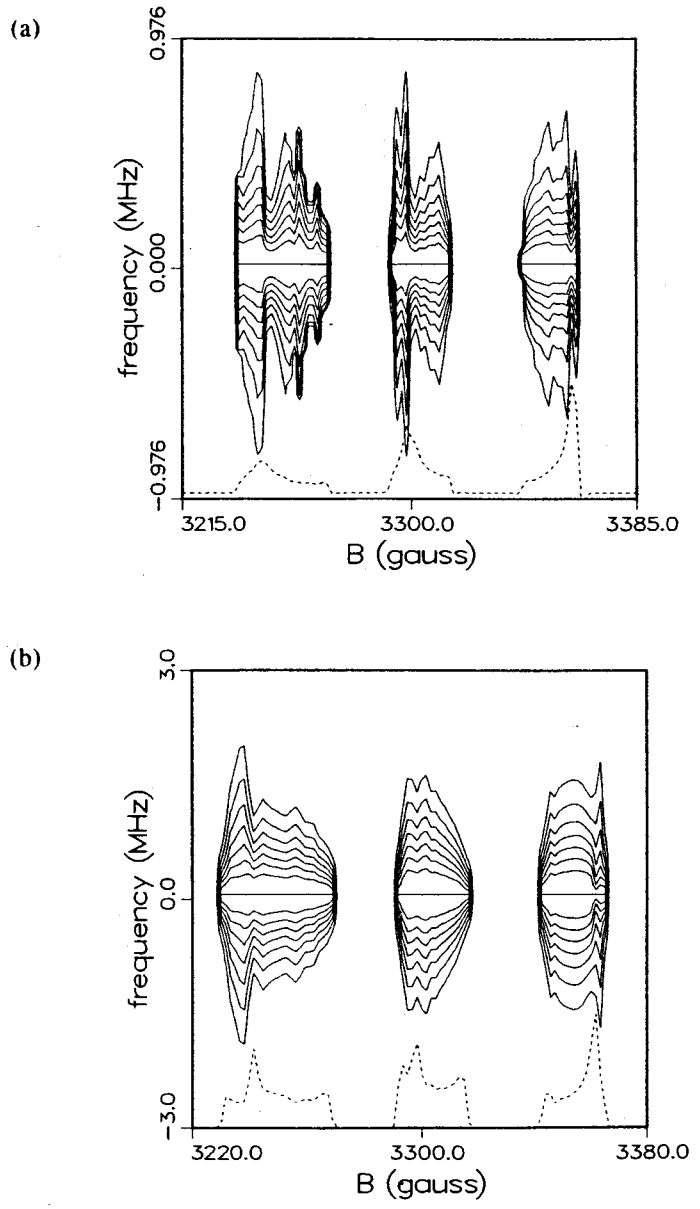

Figure 5. (a) Reconstructed 2D contours from NO_2/vycor at 35 K after removal of slowly relaxing component; (b) Calculated 2D contours for a model of anisotropic Brownian diffusion; [from (22)].

inant relaxation times T_2: a faster one of 2.5−1.2 μsec, and a slower one of 5.8−4.0 μsec. The fraction of the spectrum associated with the former increases relative to that of the latter only above 20 K (22). These results are rationalized as being due to two types of binding sites on the surface, such that the sites associated with stronger binding, hence suppressed motion, are fewer in number.

By utilizing the LPSVD method, the 2D-ESE results could be separated into the 2D spectra from two types of adsorbed NO_2. This had not been possible from the cw studies. In fact the latter showed no clear evidence for more than one type of NO_2. Further, it now became possible to interpret the observed T dependence of the cw-EPR spectrum in terms of the changing ratio of the two types of NO_2, and *not* as due to motions too slow to be observed in the inhomogeneously broadened cw-EPR spectrum! This could actually be confirmed by spectral subtraction methods (22). Furthermore it was possible to reconstruct the 2D-ESE spectrum for the more rapidly relaxing component after removal of that for the slowly relaxing component. We display the result in Figure 5a. It shows pronounced variation of T_2 across the spectrum. We are able to approximately interpret this 2D-ESE spectrum as that of anisotropic rotational diffusion about the molecular y-axis (as before) [by comparison with some simulations based on a model of anisotropic Brownian motion, *cf.* Figure 5b], but more theoretical (and experimental) work is required in order to fully clarify the motional process.

The above example clearly demonstrates the much enhanced resolution and resulting detailed information supplied by a 2D-ESE experiment. The increased resolution provided by 2D-ESE can enable one to discriminate site variations and to study the (slow) motions of the adsorbed species even though the cw-EPR spectra are too inhomogeneously broadened to enable such studies.

IV. 2D-ESE Studies of Magnetization-transfer Variations across the Spectrum

In the previous section we have demonstrated how, by the use of the standard two-pulse echo sequence, one could obtain a slow-motional 2D-ESE spectrum, which is a plot of the spectrum as a function of both the natural linewidths and the resonance positions of the DSPs. We now wish to describe an analogous experiment that is in the context of T_1 measurements, which provides a "map" of the rates of "magnetization transfer" from each spectral region. However, we must first provide the needed background on echo sequences designed to

measure T_1s and more generally "magnetization transfer." First we review (Subsection A) the standard T_1-type measurements, *i.e.*, the inversion recovery (IR) sequence π-T-$\pi/2$-τ-π-τ and the stimulated echo (SE) sequence $\pi/2$-τ-$\pi/2$-T-$\pi/2$-τ (14, 16, 19). We also summarize their theoretical interpretation in terms of motional dynamics. We then describe (Subsection B) the appropriate 2D technique and provide an example again utilizing the NO_2/vycor system.

A) *Inversion Recovery and Stimulated Echo Sequences: Full Irradiation*

The IR sequence first inverts the z-magnetization, and after a time T, the z-magnetization is probed by a simple $\pi/2$-π echo sequence. If the spectrum is fully irradiated by a "non-selective" pulse, then by stepping out T, one observes a simple exponential decay with decay constant T_1 equal to $(2w_e)^{-1}$, where w_e is the pure electron-spin-flip rate assumed, for simplicity, to be isotropic. This result is true both in the fast- and slow-motional regimes.

The SE sequence is more sophisticated. The first pulse of this sequence (called the preparation pulse) nutates the dynamic spin packets first into the x-y plane, where they precess at their individual Larmor frequencies for a time τ. During this evolution period the DSPs get out of phase, and the projection of each DSP onto the rotating y'-axis at time τ, which will be nutated onto the z-axis by the second pulse (taken as being about the x'-axis) will depend upon its Larmor frequency. In this manner, the DSPs are "frequency-labeled" during this first τ interval. During the second (i.e., T) interval (referred to as the mixing period), electron-spin flips will reduce the negative magnetization component M_z just as in the IR sequence, and this would be independent of the individual DSP labeling for an isotropic w_e. Unlike the situation in the IR sequence, motion and nuclear-spin flips will also be effective during this mixing interval. This is because, as the molecules reorient or change their nuclear-spin state, they change the DSPs to which they contribute. An echo will be formed at a time τ after the third (or detection) pulse only to the extent that the frequency labeling is still accurate at the end of the mixing interval. The more effective the motion and/or the nuclear spin flips at changing (during the mixing period) the DSPs to which a molecule contributes, the weaker will be the echo after the detection pulse.

At this point the reader may be concerned by the fact that DSPs are being "interconverted" by the molecular dynamics. Are they not the normal modes? The answer to this query lies in the fact that the DSPs as introduced above refer

to normal-mode solutions for spin-packets precessing in the rotating x'-y' plane, hence the designation of T_2-type behavior. When the spins are rotated to the (negative) z-axis, then the effective stochastic-Liouville operator (in particular the spin part) is different, so that the normal-mode solutions are different, *even though the molecular dynamics is unchanged.* These are the T_1-type normal modes (18, 19). For example, for the case of a simple g-matrix spin-Hamiltonian describing ultra-slow motion near the rigid limit, the DSPs are to a first approximation just the rigid-limit spin packets (*i.e.*, a continuum with each member representing a particular orientation), while the T_1-type normal modes are just the spherical harmonics (*i.e.*, the eigenfunctions of the simple diffusion operator which span the Hilbert space defined by the molecular orientations). This is why it is possible for the T_2-type DSPs to be interconverted during the period when T_1-type relaxation is occurring. The general theory (18, 19, 26, 27) allows one to consider the appropriate normal modes at each stage of the pulse sequence and their interconversion by each pulse.

Our theoretical results (for both $I = 0$ and $I = 1$, *e.g.*, O_2^- and NO_2 type spectra) therefore predict that the T_1-type relaxation in slow motional "magnetization-transfer" (MT) experiments may be expressed as a weighted sum of exponential decays, whose time constants represent the T_1-type normal modes. Let us call them the MT modes. The weighting factors depend, in part, on τ, which measures how long the DSPs dephase by their precession in the x-y plane after the first $\pi/2$ pulse.

As discussed above, the case of the IR sequence with full irradiation reduces to just a single exponential form

$$S(T + 2\tau) = A[1 - 2\exp(-2w_e T)], \tag{7}$$

where $S(T + 2\tau)$, the signal at time $T + 2\tau$, is that of the echo maximum and where w_e is the electron-spin relaxation rate. For SE with full irradiation, the result is written as

$$S(T + 2\tau) = \sum_p b_p(\tau)\exp(-\Lambda_{d,p}T), \tag{8}$$

where $\Lambda_{d,p}$ is the decay rate for the pth MT mode. While it would be difficult to detect many superimposed exponentials, we have found that in the limit of $w_e\tau_p \ll 1$, this expression is fit to a good approximation by a sum of only two exponential decays, *i.e.*, as

$$S(T + 2\tau) \cong A + B\exp(-2w_e T) + C\exp(-T/T_A), \tag{9}$$

where $T_A(\tau)$ is the MT time, which decreases with τ. One can show that at $\tau = 0$, $C = 0$, so there is only a single exponential decay in $2w_e$, since there is insufficient evolution time for the spins to precess appreciably in the x-y plane and the first two $\pi/2$ pulses thus add to a single π pulse. The more interesting limit is for $\tau > T_2^*$, the effective decay time of the free-induction decay (FID), (while also $\tau < T_2$), for which T_A approaches an asymptotic value such that $T_A \ll (2w_e)^{-1}$. Also B and C take on asymptotic values independent of τ that are both significant in general. In this case the frequency labeling during the evolution period is complete, so that MT during the mixing period can have its maximum effectiveness. We find this asymptotic value to be $T_A \sim \tau_R/b$ where $b \approx 2.5$ for Brownian motion and $b \approx 1$ for jump motion (18, 19). Here τ_R is the rotational correlation time. In the limit $w_e\tau_R \gg 1$ the slow motional MT is too weak, so the results are again simply described by Equation [7].

B) *2D-ESE and Magnetization Transfer: Partial Irradiation*

By analogy to the 2D technique providing T_2 variation across the spectrum, we can devise an experiment to provide the MT or T_A variation across the spectrum by employing partial irradiation. However, in the case of partial irradiation, *both* IR and SE sequences yield signals of the form of Equation [8] which are well represented by Equation [9] for all positions in the spectrum. There is now an extra MT mechanism, *viz.* MT shifting spins initially irradiated to frequencies outside the irradiated region. When this occurs, such spins are no longer detectable, and it is as though it has relaxed back to equilibrium. More precisely, spins rotated into the xy plane by the (frequency) selective preparation pulse will not even be affected by the second or mixing pulse and/or the detection pulse if they are transferred out of the irradiation "window." This mechanism is more important for IR than for SE, since in the latter case the basic spin-delabeling mechanism, described above, already supplies a closely related effect on T_A.

In summary, the relative effectiveness of MT out of the different spectral regions can be studied by such a partial irradiation technique, but first the two decays in $(2w_e)^{-1}$ and T_A^{-1} must be separated in the data processing. This is accomplished by linear prediction methods (*i.e.*, LPSVD; cf. ref. 23).

We now consider mechanisms whereby T_A can vary across the spectrum. Suppose a molecule whose principal magnetic axis is parallel to the applied field ($\theta = 0°$) makes a small Brownian jump by $\Delta\theta$. Its new spectral frequency

[1]Also note the article by J. Tang and J. R. Norris in this book.

will hardly change, because the orientation-dependent part of the resonance frequency mainly goes as $3\cos^2\theta - 1$, which for $\theta = 0°$ or $90°$ gives a change of $\Delta\omega \propto (\Delta\theta)^2$. However, for a molecule oriented at $\theta \sim 45°$, that same Brownian jump will cause a corresponding spectral frequency change given by $\Delta\omega \propto \Delta\theta$. Thus, the spin packet at the $\theta = 45°$ orientation experiences the more effective MT out of an irradiated region. Similarly if there is anisotropy of the diffusion tensor (*e.g.*, let there be rapid rotation only about the molecular *y*-axis) then DSP's associated with the perpendicular (*i.e.*, *x* and *z*) orientations will experience more rapid MT than DSPs associated with the *y*-orientation, thus yielding a greater T_A^{-1} for those DSPs associated with the perpendicular orientations.

The more general form of Equation [8] for SE with partial irradiation is (18, 19, 26, 27)

$$S(T + 2\tau) = A' e^{-2w_e T} \sum_p b_p^{\omega}(\tau) \exp(-T/\tau_p), \tag{10}$$

where

$$\tau_p^{-1} = \Lambda_{d,p}^{-1} - 2w_e \tag{11}$$

and

$$b_p^{\omega}(\tau) = \sum_{n',l',j'}^{\omega} \sum_{m,k,i} \sum_{s,q=1}^{3} O_{o,qn'} O_{o,mn'} O_{d,mp} \times O_{d,kp} O_{o,kl'} [O_{o,il'} O_{o,ij'}^*] O_{o,sj'}^* \times \exp[-(\Lambda_{o,n'} + \Lambda_{o,j'}^*)\tau]. \tag{12}$$

(For a nitroxide with 3 allowed transitions, s and q take on values 1, 2, and 3). Here O_o is the orthogonal transformation introduced in the previous section, which diagonalizes the stochastic Liouville operator associated with DSPs, and O_d is the equivalent orthogonal transformation for the MT modes. The $\Lambda_{o,n'}$ are the eigenvalues of the DSPs, while the $\Lambda_{d,r}$ are those for the MT modes. The primes appearing on the indices n', l', and j' imply that these are summed only over those DSPs which are within the irradiation window of the selective pulse, (*i.e.*, they depend upon $\omega_j - \omega$). This gives an implicit dependence upon ω as indicated. We have actually used this form for the theoretical predictions (18, 19). [In the near rigid limit, when Equation [2] applies, we may let $\Sigma_i O_{o,il'} O_{o,ij}^* \approx \delta_{l'j}$ to achieve some simplification of Equation [11]]. Fortunately, the results are approximately fit by Equation [9] at each position in the spectrum! Also, w_e is found to be constant, within experimental error, across

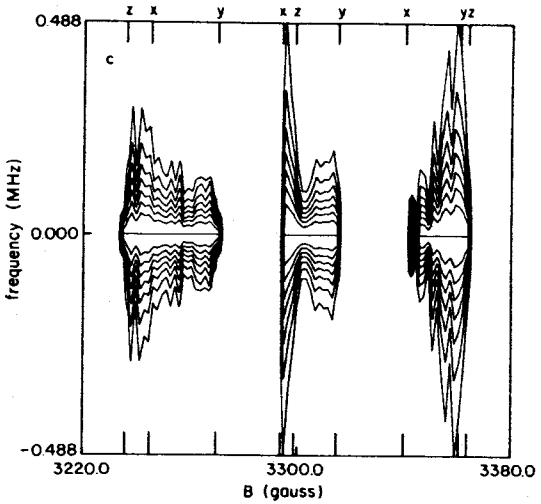

Figure 6. 2D ESE contours from the SE sequence for NO_2/vycor at 35 K. The exponential decay term in $2w_e$ (*cf.* Equation [9]) has been subtracted out [from (19)].

---

the spectrum. (But we shall encounter an expression like Equations 10−12 in Sect. VI). Thus, after extracting the term in $\exp(-T/T_A)$ by LPSVD, and after FT, one obtains a plot of $T_A/(1 + \omega^2 T_A^2)$ across the spectrum with normalized contours showing the variation of T_A.

We illustrate this 2D-MT experiment for the NO_2/vycor system discussed in the previous section. We display in Figure 6 the 2D normalized contours for T_A obtained at 35 K, where the more rapidly relaxing NO_2 species is predominant. Focussing on the $M_I = 0$ region (the central region), we see that the broadening that corresponds to the x and z molecular axes being parallel to the field is quite dramatic. This is clear evidence for more rapid rotation about the y-axis, which is consistent with the results reviewed in the previous section. The contours in the $M_I = \pm 1$ regions indicate less clear trends, probably due to inhomogeneous broadening from site variation in the hf-matrix.

This example thus indicates the potential utility of the 2D-MT experiment, which can provide useful information about molecular dynamics even before a thorough quantitative spectral analysis. Furthermore, it appears that rotational motion is detectable at lower temperatures than with the T_2-type 2D-ESE experiment described in Sect. III. The relationship to the new 2D-FT techniques will be discussed in Sect. VI.

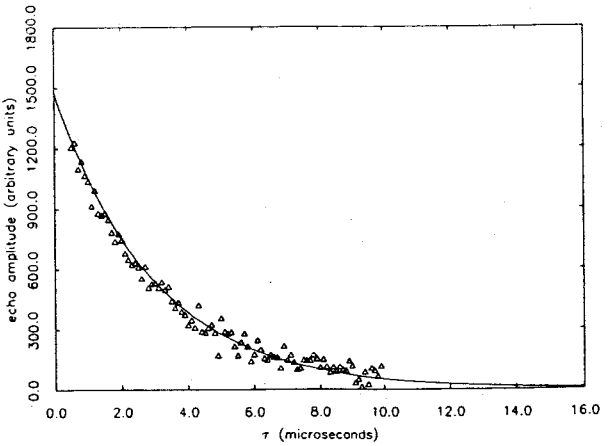

Figure 7. Experimental phase-memory decay for X-band low-field hf line of H on vycor at 5 K. The solid line is from an LPSVD fit, which yields a single exponential with $T_M = 6.2$ μs [from (22)].

V. Physisorbed Hydrogen Atoms

Hydrogen atoms physisorbed on crushed vycor can be prepared by uv irradiation of the vycor in an H_2 atmosphere at temperatures below liquid N_2 (22). The cw-EPR spectrum of the adsorbed H shows an isotropic hf splitting that is reduced by only 0.80% from that of gaseous H, demonstrating only a weak surface interaction. The spectrum shows an asymmetric lineshape which could be simulated using a very small anisotropy in $\bar{A}$: $(A_{xx}/(g_e\beta_e) = A_{yy}/(g_e\beta_e) =$ 506 G and $A_{zz}/(g_e\beta_e) = 512$ G). The hf lines are very inhomogeneous, and this is taken into account by using asymmetric broadening parameters ($T_{2_{xx}}^{*-1} = T_{2_{yy}}^{*-1} = 0.75\ \text{G} \times h/(g\beta_e)$; $T_{2_{zz}}^{*-1} = 2.2\ \text{G} \times h/(g\beta_e)$). This means that homogeneous relaxation times T_2 and T_1 cannot be measured by cw means, and that time-domain measurements are required.

By spin echo methods we found for H that $T_2 = T_M$ is 6.2 μs and is independent of temperature, hf line, H concentration, and partial pressure of H_2 (22). The phase-memory decay, T_M, is well fit by a single exponential (*cf.* Figure 7), which rules out the effect of "matrix nuclei" (28) (as does the non-dependence of T_2 on H_2 partial pressure, since adsorbed H_2 represents the predominant matrix nuclei). The non-dependence of T_2 on H concentration (22) rules out "T_2 spectral-diffusion" and "instantaneous diffusion" mechanisms (28). This value of 6.2 μs is to be compared with the previous shortest concentration-independent T_2 found for H of 40 μsec (28). The latter T_2 was

reported by Salikhov and Tsvetkov for H in mineral glasses at 77 K for [H] < 2×10^{16} cm^{-3} (28). [In our work on vycor we had [H] $\lesssim 2.5 \times 10^{15}$ cm^{-3} so that concentration-dependent relaxation effects are not to be expected]. Thus we must ask the question: if the standard solid-state-like mechanisms cannot explain our observation, is there a fundamental process or mechanism which can account for it?

Before attempting to answer this question we wish to provide further experimental "clues" (22). We note that the T_1 values for the adsorbed H decrease with T from about 0.3 s at 4.8 K to 5−10 ms at 65 K, probably due to enhanced spin relaxation produced by surface phonons present at the higher T. At any rate, since $T_1 \gg T_2$, this would rule out "T_1-spectral-diffusion", and most important it shows that the mechanism affecting T_2 does not affect T_1. Another possible mechanism would be the exchange reaction $H + H_2 \rightarrow H_2 + H$ since, every time such an exchange process occurs, there is a 50% probability that the final H is in a different nuclear spin state. This may be seen to be a special case of MT, so that we can test for it by doing an inversion-recovery (IR) experiment on one of the hf lines (*i.e.*, partial irradiation), for which an equation of form Equation [10] applies. Actually, in this simple case there are just two exponential decays such that the form of Equation [9] is valid with $T_A^{-1} = 2\omega_{ex}$, where ω_{ex} is the rate of H exchange (provided that $\omega_{ex}^{-1} < T_1$). Our IR result does yield two exponentials; one is in $T_1 = (2w_e)^{-1}$ and the other, that we tentatively assign to ω_{ex} is 80 ms at 5 K where $T_1 = 200$ ms. Since this $\omega_{ex} \ll T_2^{-1}$, the uncertainty-in-lifetime broadening from this process is much too slow to account for T_2.

There is a radiation damage signal at $g = 2$, caused by trapped electrons which can, in principle, interact with the physisorbed H. However, we estimate that the concentration is about an order of magnitude less than that of the H, so that we would not expect these impurities to be important. In fact, it is known from Tsvetkov's work on radiation damage paramagnetic species [*e.g.*, SO_4^-] that at 4.2 K the measured T_2 for H is independent of these ions even for very high concentrations of the latter (*ca.* 10^{19} cm^{-3}).

We have also produced D atoms adsorbed on crushed vycor by the same method (22). Substantially fewer D atoms are produced compared to H atoms (only about 10%). Surprisingly the T_2 values for D are about a factor of 2 shorter than those for H, and they appear to show a hf dependence such that the high-field line has a T_2 about 40% greater than that for the low-field line. Again no significant temperature dependence is observed.

We offer the following hypothesis to rationalize the above results on T_2. The

H and D atoms tunnel between different but equivalent O atoms (of SiO_2) on the surface. This would change the orientation of the O—H "van-der-Waals bond" relative to the applied static magnetic field, since the vycor has cylindrical-like pores with diameter 45−75 Å, and we can imagine the H translating within such a pore. This would yield "rotational reorientation by translational diffusion." For example, for H, let us assume that the rotational reorientation is in the slow motional regime and is approximately fit by a jump model with appreciable reorientation per tunneling jump. Then we can let $T_2 \approx \tau_c = \tau_R$ (17) [where τ_c is the mean jump time] and let $\lambda = 3$ Å (the distance between the oxygens). Then: $D = \lambda^2(4\tau_c)^{-1} \approx 5 \times 10^{-11}$ cm^2 sec^{-1}. [This value may be compared wth $D = 5 \times 10^{-12}$ cm^2 sec^{-1} for H on a tungsten surface below 150 K (29) and $1-3 \times 10^{-10}$ cm^2 sec^{-1} at 298 K for hydrogen spillover (30)].

According to such a model for the slow motional regime (17), the ratio $D_D/D_H \approx T_2(H)/T_2(D)$, a result independent of the precise magnitude (and nature) of the respective magnetic tensors and independent of hf line (17). Experimentally, we have $T_2(H)/T_2(D) > 1$ (and $T_2(D)$ dependent on hf line). This would seem to imply a reverse isotope effect. Let us suggest an alternative possibility. A tunneling jump between adjacent oxygens will, on average, cause a reorientation of only a few degrees in angle (for the above parameters). Thus, perhaps one should approximate this "rotational reorientation" as a small-angular jump. Let us assume that this is true for the D atoms. But, because H is lighter, it could tunnel directly not only to nearest neighbors, but also to next-nearest neighbors, *etc.* Thus perhaps we should use a value for $\lambda_H > \lambda_D \approx 3$ Å in our estimates such that the H atom motions involve larger "effective tunneling jumps." For very small jumps (with Brownian motion being the limit), one can show from (17) that the T_2 values predicted for the low-field and high-field lines of D would be unequal, and we estimate from the experimental result that $T_M < \tau_R \approx 20$ μsec. (This estimate is based on the A and g-matrices for D. A non-zero nuclear quadrupole term would lead to an *increased* estimated τ_R). If we let $\tau_c \approx \tau_R$, then $D_D \approx 1.1 \times 10^{-11}$ cm^2 sec^{-1}, while $D_H \approx (\lambda_H/\lambda_D)^2 \times 5 \times 10^{-11}$ cm^2 sec^{-1} or $D_D/D_H \approx 0.2\,(\lambda_D/\lambda_H)^2$ which would be less than unity, as is usually the case. Clearly, to proceed further, one must consider the quantum nature of the motion!

We believe that this example shows how time-domain EPR methods can provide useful insight into fundamental processes on surfaces.

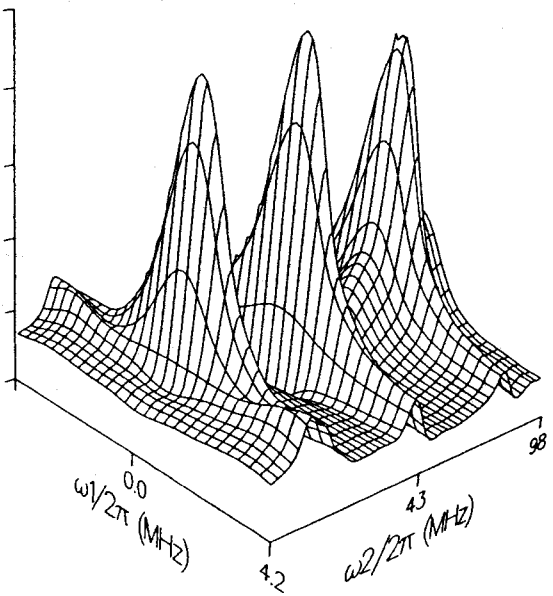

Figure 8. 2D-ESE spectrum at X-band of *ca.* 2 m<u>M</u>. PD-Tempone (perdeuterated 2,2,6,6-tetramethyl-4-piperidone *N*-oxide) in toluene-d_8 at 295 K by FT methods [from (24)].

VI. Two-dimensional Fourier-transform Techniques

We now wish to show how newly developed FT-EPR methods (31, 24) can improve and extend the range of 2D experiments on molecular dynamics. To date, this has been done for illustrative cases involving fast motional nitroxide EPR spectra, but the principles and methods can be extended to slow motions including those on surfaces. FT-EPR spectroscopy offers some instrumental challenges compared to FT-NMR. First of all the time-scale of electron spin-relaxation is of the order of nsec (compared to msec for NMR), so one must try to provide intense pulses of nsec duration. Secondly an EPR spectrum, such as that of a nitroxide, covers about 100 MHz, so that (by the Nyquist theorem) this requires time resolution of the order of at least 10 nsec with quadrature detection and narrow, intense pulses (*e.g.*, for $\gamma B_1/2\pi \sim 100$ MHz, then $B_1 \sim 36$ G and $t_p \sim 2.5$ ns). We have found that good results can be obtained with pulse widths of 5−20 ns (corresponding to $B_1 \sim 20-5$ G), which are consistent with resonators with loaded $Q \sim 100-400$, and which may be produced relatively free from jitter. These experiments require the use of a two-channel transient digitizer with good time resolution, wide frequency bandwidth, and

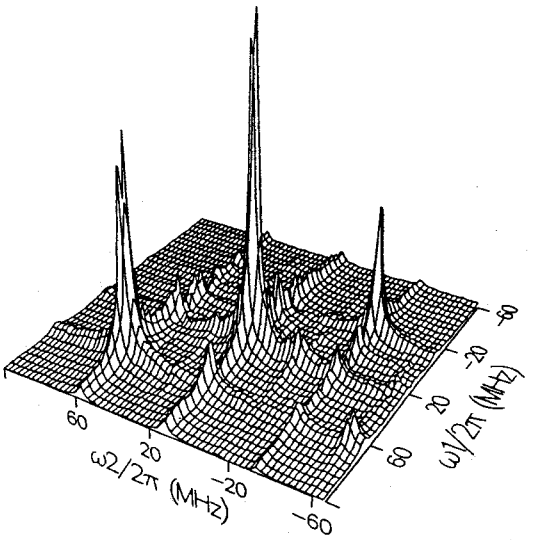

Figure 9. 2D exchange spectrum of *ca.* 2 mM PD-Tempone in toluene-d_8 at 295 K by FT methods [from (24)]. [Spurious peaks, which do *not* come at the MT peak positions, are due to incomplete image rejection, *cf.* text].

rapid repetition rates. We have used an HP54100A digital oscilloscope providing sub-nsec time resolution, 1 GHz bandwidth, and up to 1 kHz repetition rate. The two channels simultaneously receive the in-phase and out-of-phase parts of the time-domain signal provided by a quadrature detector.

The 2D-FT analogue of our field-swept T_2-type 2D-ESE experiment was illustrated in the following way. The echo after a $\pi/2$-t_1-$\pi/2$-t_1+t_2 sequence was digitized with a time resolution of 0.86 ns providing 256 complex data points, each the average of 2,048 transients. The procedure was repeated for a series of equally-spaced values of t_1 (with time resolution 6 nsec), and then was 2D-Fourier transformed. One obtains the 2D-FT-ESE spectrum shown in Figure 8 after making corrections for the fact that the irradiation field is *not* larger than the full spectral width. One observes the inhomogeneously broadened three-line hf pattern along ω_2 and the Lorentzian homogeneous lineshapes along ω_1. The field inhomogeneity was due to a small field gradient, since these fast motional lineshapes have very little natural inhomogeneity. This suppresses the FID from the second $\pi/2$ pulse. Field gradients are not necessary for a slow motional spectrum, with its substantial natural inhomogeneity, as we have seen. [There are small spurious lobes at small values of ω_2 and large

$|\omega_1|$. They are due to a combination of incomplete image rejection (*cf.* below) coupled with the amplitude and phase corrections].

By this FT procedure we are able to reduce the time required for such an experiment by an order of magnitude, and we anticipate an additional order of magnitude reduction with faster digitizers that are available.

The theory for this experiment is virtually the same as that of the field-swept 2D-ESE. Thus Equation [1] again applies with $\tau = t_1$ and $t = t_2$ (but with a_{lj} reduced by a factor of two because the second pulse is a $\pi/2$ rather than a π pulse) and is given by

$$[13] \qquad 2a_{lj} = \sum_{k,i,m} U_k O_{kl} V_l O_{il} O_{ij}^* V_j^* O_{mj}^* U_m^*.$$

The V_l give the correction for variation of effective B_1 across the spectrum, i.e., the lth DSP resonanting at angular frequency ω_l experiences an effective rotation that depends on $\omega_l - \omega$ (with ω the irradiating frequency) and on B_1 (31). Then FT with respect to $2t_1$ and t_2 gives

$$[14] \qquad S(\omega_1, \omega_2) = \sum_{l,j} a_{lj} \left| \frac{1}{i\omega_1 - \frac{1}{2}(\Lambda_l + \Lambda_j^*)} \right| \left| \frac{1}{i\omega_2 - \Lambda_l} \right|.$$

Thus inhomogeneous broadening is removed along the ω_1 axis.

We now give an example of a 2D-FT experiment that displays the effects of MT. More precisely, it is a way of performing electron-electron double resonance (ELDOR) but with only a single frequency source! The spectral band produced by a finite pulse is coherently related, and this is the basis for the power of the technique. It is based upon the $\pi/2$-t_1-$\pi/2$-T-$\pi/2$-t_2 Jeener–Ernst pulse sequence (32) which involves the four time periods: preparation, evolution, mixing, and detection (*cf.* Sect. IV).

The preparation period consists of a $\pi/2$ pulse to generate the initial transverse magnetization. The phase of this pulse determines the phase of the amplitude modulation that results from the "frequency labeling" during the subsequent evolution period of duration t_1. The second $\pi/2$ pulse marks the beginning of the mixing period wherein the longitudinal magnetization components associated with each hf line can be exchanged, thereby mixing components carrying different precessional-frequency information (*i.e.*, MT occurs). Thus, after rotating this magnetization into the xy plane for detection, components initially precessing with angular frequency $\omega_1 = \omega_a$ will (to the extent that MT occurred by exchange during the mixing period) precess with

new frequency $\omega_2 = \omega_b$. In our example, shown in Figure 9, we rely on the appreciable Heisenberg spin-exchange (HE) (33, 34) to produce the MT between the hf lines (18).

The pulse sequence is repeated for a series of equally spaced values of t_1. For each t_1 the FID is collected, then the phase of the preparation pulse is advanced by 90°, and a second FID is collected. The two FID data sets are stored in separate files [call them $S'(t_1, t_2)$ and $S''(t_1, t_2)$]. It is easy to show that these two signals depend on terms oscillatory in t_1 that are in phase quadrature (35). FT of each data set with respect to t_2 yields the intermediate results $|S'(t_1, \omega_2)|$ and $|S''(t_1, \omega_2)|$. After further processing [including suppression of the contribution of the "axial peaks" (36)] the two *real* data records are combined to form a new *complex* one, i.e., $S(t_1, \omega_2) = |S'(t_1, \omega_2)| + i|S(t_1, \omega_2)|$, which yields the desired 2D spectrum $|S(\omega_1, \omega_2)|$ upon final FT.

This technique of phase alternation supplies the phase information necessary to obtain the pure absorption 2D spectrum. It should be particularly useful for cases of slow-tumbling motion on surfaces for which the spectra are composed of very many DSPs (*cf.* Sect. IV). For such systems the 2D spectrum would lead to direct correlation of the MT between DSPs from the different molecular orientations!

In our fast-motional example in Figure 9, the diagonal peaks correspond to the three ^{14}N hf lines, while the (six) off-diagonal peaks (where the values of ω_1 and ω_2 correspond to different hf frequencies) represent MT from one line to the other. They are the "ELDOR peaks" as described below. These results are consistent with the theory below, that is applicable for the present case of the HE rate being comparable to electron-spin relaxation (37, 38). Some spurious peaks, which do *not* come at the MT-peak positions, are due to imperfections in the quadrature detector, (*i.e.*, imperfect image rejection). It is a virtue of the 2D technique that it allows one to separate out (or "frequency discriminate") such peaks from the relevant peaks. One can guarantee that they do not interfere with the MT peaks by setting the microwave frequency to be displaced from the center of the spectrum. New phase cycling schemes show promise in eliminating problems due to imperfect image rejection. Also, there is an additional contribution, *only* to the diagonal peaks (*i.e.*, those peaks for which $\omega_1 = \omega_2$), from the transverse magnetization generated by the first pulse which continues to freely precess for the rest of the sequence. This additional contribution should be eliminated by a pulsed field-gradient technique (32) analogous to that used (39) to step the magnetic field or by a phase cycling scheme (40). Figure 9 is based upon 70 values of t_1 (*i.e.*, 140 FID experi-

ments), with a total acquisition time of 20 minutes, or about 8.6 sec per signal averaged FID.

The theory for this experiment yields the echo intensity written as:

$$[15] \qquad S(t_1 + T + t_2) = B' \sum_{p,n',j'} c_{p,n',j'} \exp(-T/\tau_p) \exp(-\Lambda_{o,n'} t_2) \times \exp(-\Lambda_{o,j'} t_1)$$

with

$$[16] \qquad c_{p,n',j'} = \sum_{q,m,k,l',i,s} U_q O_{o,qn'} V_{n'} O_{o,mn'} O_{d,mp} O_{d,kp} \times (O_{o,kl'} V_{l'} O_{o,il'} O_{o,ij'}) V_{j'} O_{o,sj'} U_s$$

This expression is very similar to that of Equation [12] for the field-swept 2D-ESE experiment, except for the fact that an FID (rather than an echo is detected), and we have explicitly included the V vector which, as noted above, includes the effects of an effective B_1 that varies across the spectrum. To obtain the 2D spectrum we FT the complex exponentials in t_1 and t_2 as in Equation [4] above. In particular, in the case of Figure 9, corresponding to the motionally-narrowed regime with three well-separated EPR lines, we can write our expressions as

$$[17] \qquad S(T, \omega_1, \omega_2) = B' \sum_{k,j',n'} U_{n'} V_{n'} \left| \frac{1}{i\omega_1 - \Lambda_{n'}} \right| U_{j'} V_{j'}^2 \left| \frac{1}{i\omega_2 - \Lambda_{j'}} \right| \times O_{d,n'p} O_{d,j'p} \exp[-T/\tau_p]$$

with

$$[18] \qquad O_{d,n'p} = \begin{array}{c} \begin{array}{ccc} \underline{1} & \underline{2} & \underline{3} \end{array} \\ \begin{pmatrix} 3^{-1/2} & 2^{-1/2} & 6^{-1/2} \\ 3^{-1/2} & 0 & -2(6^{-1/2}) \\ 3^{-1/2} & -2^{-1/2} & 6^{-1/2} \end{pmatrix} \end{array} \begin{array}{c} -1 \\ 0 \\ 1 \end{array}$$

and with $n' = M_I = -1, 0, 1$ and $\tau_1^{-1} = 2w_e$, $\tau_2^{-1} = 2w_e + w_n + \omega_{HE}$, and $\tau_3^{-1} = 2w_e + 3w_n + \omega_{HE}$ (26, 27). Here ω_{HE} is the rate of HE and w_n is the nuclear-spin-flip rate. Thus, for example, the $M_I = 0$ diagonal peak decays in T as $1/3 \exp(-2w_eT) + (2/3) \exp[-(2w_e + 3w_n + \omega_{HE})T]$, while the cross-peak or "ELDOR line" corresponding to $n' = +1$ and $j' = 0$ exhibits the T dependence $(1/3)\{\exp(-2\omega_eT) - \exp[-(2w_e + 3w_n + \omega_{HE})T]\}$ which is an ELDOR effect! Note that the relative amplitudes of peaks and cross-peaks require the correction $V_{n'} V_{j'}^2$, so they are not necessarily known accurately. On the other hand, a sequence of such 2D spectra for various T can be fit, for each peak, to the expressions in T to obtain the various decay terms. In this way an

ELDOR experiment may be performed simultaneously for all ELDOR lines. Equations [15] and [16] are applicable to slow motional spectra, and this 2D-FT experiment would give a direct display of the reorientational process. Also, one could monitor the SE instead of the FID if the FID decays too rapidly (*i.e.*, $T_2^* \lesssim \tau_d$).

In summary, these new 2D-FT techniques, as they are perfected, may be expected to play a very important role in the study of slow motions on surfaces and of slow motions in general.

VII. Acknowledgements

We gratefully acknowledge the support of this research by NSF Grant No. CHE83-19826, by the Cornell Materials Science Center (NSF), and by NIH Grant No. GM25862.

References

1. G. M. Muha. J. Phys. Chem. **71**, 633, 640 (1967).
2. G. B. Garbutt, H. D. Gosser and M. Fujimoto. J. Chem. Phys. **48**, 4605 (1968).
3. M. Iwaizumi, S. Kubota and T. Isobe. Bull. Chem. Soc. Jpn. **44**, 3227 (1971).
4. T. Komatsu and A. Lund. J. Phys. Chem. **76**, 1727 (1972).
5. M. Shiotani, F. Yuasa, and J. Sohma. J. Phys. Chem. **79**, 2669 (1975).
6. J. Sohma and M. Shiotani. Magnetic Resonance in Colloid and Interface Science, ACS Symposium Series **34**, Edited by H. A. Resing and C. G. Wade, (ACS, Washington, D.C., 1976), p. 141.
7. M. Che and A. J. Tench. Adv. Catal. **32**, 1 (1983).
8. T. M. Pietrzak and D. E. Wood. J. Chem. Phys. **35**, 2454 (1970).
9. R. B. Clarkson and R. G. Kooser. Surf. Sci. **74**, 325 (1978).
10. S. Schlick and L. Kevan. J. Phys. Chem. **83**, 3424 (1979); J. Chem. Phys. **72**, 784 (1980); J. Am. Chem. Soc. **102**, 4622 (1980).
11. M. Shiotani, G. Moro, and J. H. Freed. J. Chem. Phys. **74**, 2616 (1981).
12. M. Shiotani and J. H. Freed. J. Phys. Chem. **85**, 3873 (1981).
13. K. M. Salikhov, A. G. Semenov, and Yu. D. Tsvetkov. Electron Spin Echoes and Their Applications (Nauka, Novosibirsk, 1976).
14. L. Kevan and R. N. Schwartz. eds. Time Domain Electron Spin Resonance (Wiley-Interscience, NY 1979).
15. J. R. Norris, M. C. Thurnauer, and M. K. Bowman. Adv. Biol. Med. Phys. **17**, 365 (1980).
16. A. E. Stillman and R. N. Schwartz. J. Phys. Chem. **85**, 3031 (1981).
17. L. J. Schwartz, A. E. Stillman and J. H. Freed. J. Chem. Phys. **77**, 5410 (1982).
18. L. J. Schwartz. Ph.D. Thesis, Cornell University (1984).
19. L. J. Schwartz, G. L. Millhauser and J. H. Freed. Chem. Phys. Lett. **127**, 60 (1986).
20. G. L. Millhauser and J. H. Freed. J. Chem. Phys. **81**, 37 (1984).
21. L. Kar, G. L. Millhauser, and J. H. Freed. J. Phys. Chem. **88**, 3951 (1984).
22. G. L. Millhauser. Ph.D. Thesis, Cornell University (1986).
23. G. L. Millhauser and J. H. Freed. J. Chem. Phys. **85**, 63 (1986), and references therein.
24. J. Gorcester and J. H. Freed. J. Chem. Phys. **85**, 5375 (1986).
25. K. Tatsumi, M. Shiotani, and J. H. Freed. J. Phys. Chem. **87**, 3425 (1983).
26. J. H. Freed. J. Phys. Chem. **78**, 1155 (1974).

27. J. H. FREED. *In* Time Domain Electron Spin Resonance. Ch. 2. Edited by L. Kevàn and R. N. Schwartz. Wiley Interscience, New York, 1979.
28. K. M. SALIKHOV and YU. D. TSVETKOV. *In* Time Domain Electron Spin Resonance. Ch. 7. Edited by L. Kevan and R. N. Schwartz.
29. R. DIFOGGIO and R. GOMER. Phys. Rev. B**25**, 3490 (1982).
30. R. V. DMITRIEV, K. H. STEINBERG, A. N. DETJUK, F. HOFMANN, H. BREMER, and KH. M. MINACHEV. J. Catal. **65**, 105 (1980).
31. J. P. HORNAK and J. H. FREED. J. Magn. Reson. **67**, 501 (1986).
32. J. JEENER, B. H. MEIER, P. BACHMANN and R. R. ERNST. J. Chem. Phys. **71**, 11 (1979).
33. J. H. FREED. J. Chem. Phys. **45**, 3452 (1966).
34. M. P. EASTMAN, R. G. KOOSER, M. R. DAS and J. H. FREED. J. Chem. Phys. **51**, 2690 (1969).
35. J. KEELER and D. NEUHAUS. J. Magn. Reson. **63**, 454 (1985).
36. W. P. AUE, E. BARTHOLDI and R. R. ERNST. J. Chem. Phys. **64**, 2229 (1976).
37. J. S. HWANG, R. P. MASON, L. P. HWANG and J. H. FREED. J. Phys. Chem. **79**, 489 (1975).
38. R. N. SCHWARTZ, L. L. JONES and M. K. BOWMAN. J. Phys. Chem. **83**, 3429 (1979).
39. J. P. HORNAK and J. H. FREED. Chem. Phys. Lett. **101**, 115 (1983).
40. S. MACURA and R. R. ERNST. Mol. Phys. **41**, 95 (1980).